Possible halo structure of ^{62,72}Ca by forbidden-state-free locally peaked Gaussians

W. Horiuchi [1,*] Y. Suzuki,[2,3] M. A. Shalchi,[4] and Lauro Tomio[4]

[1]*Department of Physics, Hokkaido University, Sapporo 060-0810, Japan*
[2]*Department of Physics, Niigata University, Niigata 950-2181, Japan*
[3]*RIKEN Nishina Center, Wako 351-0198, Japan*
[4]*Instituto de Física Teórica, Universidade Estadual Paulista, 01140-070 São Paulo, São Paulo, Brasil*

In order to efficiently describe nucleon orbits around a heavy core nucleus, we propose locally peaked Gaussians orthogonalized to the occupied bound states in the core. We show the advantage of those functions in both numerical stability and fast convergence by taking examples of touchstone calcium isotopes ^{62,72}Ca in ^{60,70}Ca $+n+n$ three-body models. Both weakly bound configurations and continuum coupling effect are taken into account. We evaluate the neutron radii and the occupation probabilities of two-neutron configurations not only for the ground state but also for some particle-bound excited states by varying the strength of the core-neutron interaction. The emergence of the halo structure in the ground state depends on the energy difference between $2s_{1/2}$ and $0g_{9/2}$ orbits. Two-neutron [consisting of $(s_{1/2})^2$ configuration] and one-neutron [consisting of $(g_{9/2}s_{1/2})$ configuration] halo structures of ^{62}Ca can coexist in narrow energy spacing provided that both of $2s_{1/2}$ and $0g_{9/2}$ orbits are almost degenerate and barely bound. The ground-state structure of ^{72}Ca is likely to be a two-neutron halo, although its emergence depends on the position of the $2s_{1/2}$ level.

I. INTRODUCTION

The landscape of exotic short-lived nuclei far from the stability line extends to the neutron dripline up to Ne isotopes [1]. In such extreme neutron excess, weakly bound neutrons emerge and often lead to neutron-halo structure. Exploring the halo nuclei has continued since the first discovery of the two-neutron halo nucleus ^{11}Li [2]. Other typical examples of two-neutron halo nuclei include ^{6}He [2], ^{14}Be [3], ^{19}B [4], and ^{22}C [5–7]. See also Ref. [8] for more experimental and theoretical references on halo-nuclei studies. Recently, by measuring its interaction cross section, ^{29}F has been identified as the heaviest two-neutron halo nucleus [9].

The two-neutron halo structure has often been described using a core plus two-neutron model. When the core is a light nucleus, the two-neutron motion can be accurately described, e.g., as in ^{22}C [5]. Within the search for evidence of Efimov states [10] in two-neutron ($2n$) halo nuclei close to the neutron-core (n-core) unitary limit [11,12], the emergence of universal properties described by two-body observables and a three-body scaling parameter became quite clear in the case of two neutrons bound to light-core nuclei.

Motivated by the recent measurement reported in Ref. [9], the dripline and near-dripline F isotopes have been studied by three-body models: For ^{29}F, the p-wave two-neutron halo character of ^{27}F $+n+n$ was verified in Refs. [13–15], and

a competition of halo and antihalo configurations was proposed in Ref. [16] for ^{31}F studied as ^{29}F $+n+n$. By using the Gamow shell model these F isotopes were also studied in Ref. [17]. Studying the existence of heavier neutron-halo nuclei is interesting as it will help to expose the binding mechanism when increasing the mass number [18,19], which opens the possibility of verifying universal aspects expected to emerge in low-energy quantum systems, such as ultracold atom-molecule heteronuclear systems [12,20,21]. However, a microscopic description becomes tougher as the core nucleus becomes heavier because the number of the occupied orbits in the core increases. Therefore, a reliable and efficient method is needed to describe the two-neutron motion around the heavy core nucleus. The complication of such calculation is mainly due to the condition that requires the configuration space available to the valence neutrons to be orthogonal to all the bound states occupied in the core (orthogonality condition model [22,23]). To eliminate such bound states (called forbidden states) from a three-body solution, a pseudopotential method [24] has often been applied. With increasing the mass number of the core nucleus, the number of the occupied orbits increases and the description of the valence neutron orbits becomes more complicated and often numerically unstable.

To describe the nucleon motion around the core, one can use explicitly correlated Gaussians [25–27]. Due to the complexity of removing the forbidden states, however, its application is limited only to light nuclei. See, e.g., Refs. [28,29]. Obviously, a single-particle (sp) basis is advantageous to eliminate the forbidden state. The application of Gaussian sp basis functions to the alpha decay of ^{212}Po

---
*whoriuchi@nucl.sci.hokudai.ac.jp

in the ^{208}Pb $+n+n+p+p$ model was in fact successfully made in Ref. [30]. It turned out, however, that the description was not perfect for the localized nucleon orbits, i.e., the alpha clustering near the nuclear surface. This is probably because the ordinary Gaussians, $r^l \exp(-ar^2)$, used there are not always enough to obtain large amplitude near the nuclear surface. In Refs. [31,32], locally peaked Gaussians (LPGs), $r^{2k+l} \exp(-ar^2)$, are proposed to describe the localized configurations. By the additional r^{2k} factor, the LPG basis allows one to describe not only damped short-ranged behavior [25,26] but also large amplitude far from the center, while keeping the advantage that the matrix elements of the LPG bases can easily be evaluated.

In this paper, we introduce a forbidden-state-free LPG (FFLPG) to efficiently describe neutron orbits around a heavy core nucleus. This opens up the perspectives to study more complicated multinucleon systems around the heavy core. To show its effectiveness, we apply the method to describe ^{62,72}Ca in which the emergence of the two-neutron halo was discussed [18,19]. The purpose of this paper is twofold: (1) to establish an efficient way to describe both the short-ranged nodal behavior and enhanced amplitude beyond the nuclear surface, which is expected to occur in nucleon orbits around the heavy core, and (2) to clarify the conditions under which halo structure can emerge not only in the ground state but also in some excited states of the ^{60,70}Ca $+n+n$ three-body systems.

As mentioned above, we focus on the neutron-rich Ca isotopes having large number N of neutrons. Although the halo structure is expected to appear for $N > 40$, its structure or even its existence is under debate. Very little experimental information is available for the Ca isotopes: The heaviest, ^{60}Ca, was confirmed in Ref. [33] but no information other than its existence is available. Mass measurements have been done up to ^{57}Ca [34], and the charge radii [35] have been determined up to ^{52}Ca, and recently interaction cross sections have been measured up to ^{51}Ca [36]. It was conjectured by the coupled-cluster calculation that the neutron dripline of Ca isotopes is around ^{60}Ca [37] and ^{62}Ca has two-neutron halo structure with dominant s wave [18]. On the other hand energy-density-functional [38,39], shell-model [40], and in-medium similarity renormalization group [41] calculations predicted that the dripline is around ^{70}Ca. The halo structure of ^{72}Ca was also predicted by the relativistic mean-field model [42]. The two-neutron halo structure in the ground state of ^{72}Ca and its relationship to the Efimov physics was studied by a ^{70}Ca $+n+n$ model [19]. The dripline of Ca isotopes was predicted to be ^{72}Ca based on a Bayesian analysis of the density functional theory results [43]. Since there is still some ambiguity in determining the dripline, we leave its question open and study possible neutron-halo structure in the spectrum of both cases, ^{62,72}Ca.

The paper is organized as follows. Section II presents the Hamiltonian and some definitions needed to introduce the present approach and explains how to construct the FFLPG. Section III discusses our results. First, in Sec. III A the Ca $+ n$ potential employed in this paper is investigated. Section III B is devoted to test the power of this approach to the ^{60}Ca $+n+$

n system. Comparison with a standard projection method is presented. Section III C discusses the emergence of various halo structures in the spectrum of ^{62}Ca based on the three-body results. The case of ^{72}Ca is presented in Sec. III D. Conclusions and future perspectives are given in Sec. IV.

II. FORMULATION

A. Hamiltonian and variational calculation

The Hamiltonian of a core+2n system consists of the n-core kinetic (T) and potential (U) and the n-n potential (v) terms,

$$H = \sum_{i=1}^{2} (T_i + U_i) + \frac{1}{Am_N} \boldsymbol{p}_1 \cdot \boldsymbol{p}_2 + v_{12}, \quad (1)$$

where m_N and A are the nucleon mass and the mass number of the core nucleus, respectively. We follow the cluster-orbital shell model approach [44], by reducing the three-body problem to a two-body problem using two independent n-core relative distance vectors, $\boldsymbol{r}_1$ and $\boldsymbol{r}_2$ with their respective momentum conjugates $\boldsymbol{p}_1$ and $\boldsymbol{p}_2$. The center-of-mass kinetic energy is subtracted and the corresponding kinetic energies are given by $T_i = \boldsymbol{p}_i^2/(2\mu)$ with $\mu = m_N A/(A + 1)$. Our choices for the n-core and n-n potentials will be given later.

The total wave function with the angular momentum J and its z component M is expanded in terms of K basis functions $\Phi_{JM}(\alpha_i)$ ($i = 1, \ldots, K$):

$$\Psi_{JM} = \sum_{i=1}^{K} c_i \Phi_{JM}(\alpha_i), \quad (2)$$

where α_i denotes a set of variational parameters for the ith basis. These basis functions are not restricted to be orthogonal. A set of linear coefficients $\boldsymbol{c} = (c_1, \ldots, c_K)^t$ is determined variationally by solving the generalized eigenvalue problem

$$\mathcal{H}\boldsymbol{c} = E\mathcal{B}\boldsymbol{c}, \quad (3)$$

where $\mathcal{H}$ and $\mathcal{B}$ are the Hamiltonian and overlap matrices with elements defined by

$$\mathcal{H}_{ij} = \langle \Phi(\alpha_i)|H|\Phi(\alpha_j) \rangle \quad (4)$$

and

$$\mathcal{B}_{ij} = \langle \Phi(\alpha_i)|\Phi(\alpha_j) \rangle. \quad (5)$$

An optimal set of α_i is selected by the stochastic variational method (SVM) [25,26]. Its efficiency was demonstrated by a number of examples. See, e.g., Refs. [27,28,45]. We increase the basis one by one by selecting the one that gives the lowest energy among randomly generated candidates until the energy convergence is met. This procedure greatly reduces the total number of basis K, which helps the description of nucleon systems around a heavy core, where the number of possible configurations is quite large.

B. Definition of FFLPG

The efficiency of a variational calculation strongly depends on a choice of basis functions. Some basic requirements for a "good" basis include the following in the present case:

(i) Weaklybound neutron orbits should be well described, because the system may have large amplitude at and beyond the surface of the core nucleus. (ii) The evaluation of the matrix elements in Eqs. (4) and (5) should be easy and extendable to systems with more neutrons bound to the core. (iii) The removal of many forbidden states should be performed numerically easily and stably.

The sp wave function with total (orbital) angular momentum j (l), with their corresponding angular and spin wave functions, $Y_l(\hat{r})$ and $\chi_{1/2}$, is defined by

$$\phi^a_{kljm} = \phi^a_{kl}(r)[Y_l(\hat{r})\chi_{1/2}]_{jm}, \tag{6}$$

where the LPG function is given by

$$\phi^a_{kl}(r) = N_{kl}\left(\frac{a^3}{\pi}\right)^{\frac{1}{4}}(\sqrt{a}\,r)^{2k+l}\exp\left(-\frac{1}{2}ar^2\right), \tag{7}$$

Here, N_{kl} is the normalization constant

$$N_{kl} = \sqrt{\frac{2^{2k+l+2}}{(4k+2l+1)!!}}, \tag{8}$$

and a is a parameter related to the width of the LPG function. We assume k to be a non-negative integer for the sake of simplicity. The LPG with $k=0$ is nothing but the ordinary Gaussians. Most of basic matrix elements between the LPG bases can be obtained analytically [31]. Since the LPG reaches a maximum at $r = \sqrt{(2k+l)/a}$, a suitable combination of a and k can describe such wave packets that are centered at different positions and have different widths. Because of this flexibility, the LPG can describe even linear chain structure [31]. Obviously the tail of a weakly bound orbit can be described well by a superposition of the LPG. This flexibility is vital to describe the sp orbits around a heavy core nucleus.

The LPG basis satisfies the requirements (i) and (ii). Concerning the requirement (iii), we introduce a projection operator onto the forbidden (F) space,

$$P_F = \sum_{n'l'j'\in F}\sum_{m'=-j'}^{j'}|\psi_{n'l'j'm'}\rangle\langle\psi_{n'l'j'm'}|, \tag{9}$$

where the sum extends over all the orbits occupied in the core nucleus. The forbidden states ψ_{nljm} are defined by the bound-state solutions of the one-body Hamiltonian, $T + U$. As will be seen later, they are very well approximated by the harmonic-oscillator (HO) functions

$$\psi^\nu_{nljm} = \psi^\nu_{nl}(r)[Y_l(\hat{r})\chi_{1/2}]_{jm} \tag{10}$$

with the principal quantum number (n) and an appropriately chosen oscillator parameter ν. We use this approximation in what follows. The FFLPG sp orbit is defined by

$$\begin{aligned}
\bar{\phi}^a_{kljm} &= (1 - P_F)\phi^a_{kljm} \\
&= \phi^a_{kljm} - \sum_{n';n'lj\in F}\langle\psi^\nu_{n'l}|\phi^a_{kl}\rangle\psi^\nu_{n'ljm} \\
&\equiv \bar{\phi}^a_{kl}(r)[Y_l(\hat{r})\chi_{1/2}]_{jm}.
\end{aligned} \tag{11}$$

Because $\psi^\nu_{n'l}(r)$ is a combination of LPG's, $\phi^\nu_{k'l}(r)$ ($k' = 0, \ldots, n'$), $\langle\psi^\nu_{n'l}|\phi^a_{kl}\rangle$ is readily obtained by using

$$\begin{aligned}
\langle\phi^{a'}_{k'l}|\phi^a_{kl}\rangle &= \frac{(2k+2k'+2l+1)!!}{\sqrt{(4k+2l+1)!!(4k'+2l+1)!!}} \\
&\times \frac{\sqrt{a}^{2k+l+\frac{3}{2}}\sqrt{a'}^{2k'+l+\frac{3}{2}}}{(\frac{a+a'}{2})^{k+k'+l+\frac{3}{2}}},
\end{aligned} \tag{12}$$

which leads to easy determination of $\bar{\phi}^a_{kljm}$.

With the use of the sp basis defined above, we construct an antisymmetrized two-neutron basis

$$\begin{aligned}
&\Phi_{JM}(a_1k_1l_1j_1; a_2k_2l_2j_2) \\
&= \frac{1}{\sqrt{2}}(1 - P_{12})\left\{\left[\bar{\phi}^{a_1}_{k_1l_1j_1}(1)\bar{\phi}^{a_2}_{k_2l_2j_2}(2)\right]_{JM}\right\},
\end{aligned} \tag{13}$$

where P_{12} exchanges the neutron labels 1 and 2, and $[j_1j_2]_{JM}$ denotes the tensor product. Here, the set of variational parameters of the ith basis α_i in Eq. (2) stands for $\alpha_i = (a_{1,i}k_{1,i}l_{1,i}j_{1,i}, a_{2,i}k_{2,i}l_{2,i}j_{2,i})$. This two-neutron basis can easily be extended to core+few-nucleon systems by successively coupling another nucleon one by one.

Note that the variational parameter α_i comprises eight variables: two continuous ones ($a_{1,i}$ and $a_{2,i}$) and six discrete ones. As will be shown later, both of short- and long-ranged LPG's have to be superposed to properly describe the asymptotics of the FF halo wave functions and also continuum states with high angular momenta ($l_{1,i}$ and $l_{2,i}$) have to be included to reach convergence. Therefore, discretizing each component of α_i on certain grids would lead to enormous basis dimension even for the present three-body system. More crucial is that one has to take into account the possibility of producing two bound states with the same spin and parity. A way to overcome these difficult problems is to reduce the basis dimension by the SVM. An interested reader should refer to Chapter 4 of Ref. [26].

The above basis of Eq. (13) is completely FF. In contrast to this approach, a popular way of eliminating the forbidden components is to add a pseudopotential to the Hamiltonian as in Ref. [24],

$$H \rightarrow H + \lambda\sum_{i=1}^{2}P_F(i), \tag{14}$$

and to attempt at reaching a stable eigenvalue by taking $\lambda \rightarrow \infty$. In practice, $\lambda \approx 10^4$ MeV is taken [28]. This pseudopotential method has the advantage of its simplicity. We compare both approaches in the next section.

III. APPLICATION TO Ca + n + n SYSTEMS

A. Choice of n-^{60}Ca potential

We take the Woods-Saxon (WS) form for the n-^{60}Ca potential

$$U(r) = -V_0 f_{\text{WS}}(r) + V_1 r_0^2 \frac{1}{r}\frac{df_{\text{WS}}(r)}{dr}(\boldsymbol{\ell}\cdot\boldsymbol{s}), \tag{15}$$

where $f_{\text{WS}}(r) = [1 + \exp(r - R_{\text{WS}})/a_{\text{WS}}]^{-1}$ with $R_{\text{WS}} = r_0 A^{1/3}$ and $r_0 = 1.27$ fm. We use two sets for the diffuseness
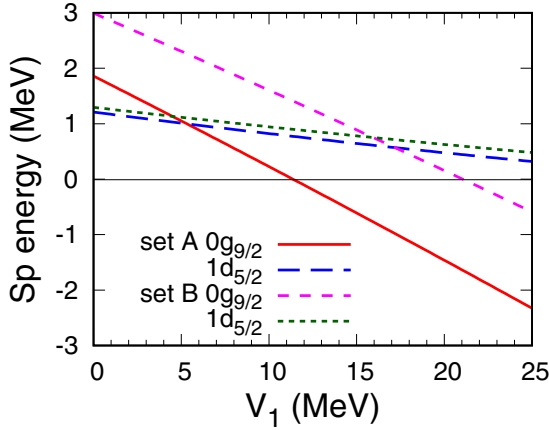
FIG. 1. Single-particle energies of $0g_{9/2}$ and $1d_{5/2}$ orbits of ^{61}Ca as a function of the spin-orbit strength V_1. The diffuseness parameter, a_{WS}, is 0.67 fm for set A and 0.80 fm for set B. The $2s_{1/2}$ sp energy, independent of V_1, is set to -0.01 MeV, as indicated by the thin horizontal line.

parameter: One is a standard one, $a_{\mathrm{WS}} = 0.67$ fm (set A), and the other is a larger one, $a_{\mathrm{WS}} = 0.80$ fm (set B).

The ^{60}Ca core nucleus is assumed to have the $N = 40$ closed configuration, that is, the occupied orbits include $0s_{1/2}$, $0p_{3/2}$, $0p_{1/2}$, $1s_{1/2}$, $0d_{5/2}$, $0d_{3/2}$, $1p_{3/2}$, $1p_{1/2}$, $0f_{7/2}$, $0f_{5/2}$. We generate these forbidden states by assuming the WS potential parameters of Eq. (2-182) in Ref. [46]. Those potential parameters are $V_0 = 40.00$ MeV and $V_1 = 17.60$ MeV. Note that the potential makes both of $0g_{9/2}$ and $2s_{1/2}$ orbits unbound. The HO parameter ν is determined so as to maximize the average of the squared overlaps, $\sum_{nljm \in F} \langle \psi_{nljm} | \psi^{\nu}_{nljm} \rangle^2 / 40$ (see Ref. [47]). The maximum average value is 0.988 for set A and the resulting ν value is 0.212 fm^{-2}, while in set B case they are 0.989 and 0.203 fm^{-2}. Approximating the forbidden states with the HO wave functions is quite reasonable.

There is no information about ^{61}Ca. Even its stability is unknown. The valence neutron orbit of ^{61}Ca belongs to the $2n + l = 4$ shell comprising the $0g$, $1d$, and $2s$ orbits. The order of these sp orbits is under debate [19,38–43]. The standard shell-model filling with the spin-orbit interaction arranges the sp levels in the order of $0g_{9/2}$, $2s_{1/2}$, and $1d_{5/2}$ at $A \approx 60$ [46], while Ref. [37] predicted the inverted order of $2s_{1/2}$, $1d_{5/2}$, and $0g_{9/2}$. In the latter case, the halo structure would appear in the ground state of ^{62}Ca [18]. Following this inverted situation, we determine V_0 in Eq. (15) so as to set the $2s_{1/2}$ sp energy to be -0.01 MeV, resulting in $V_0 = 44.03$ MeV (set A) and 41.89 MeV (set B), respectively. The value turns out to be slightly stronger than the standard value $V_0 \approx 40$ MeV [46].

We vary the spin-orbit strength V_1 in Eq. (15) to simulate different conditions for the ^{61}Ca structure. Figure 1 plots the sp energies of the $0g_{9/2}$ and $1d_{5/2}$ orbits. Note that the standard value of V_1 for ^{60}Ca is $0.44V_0 \approx 19$ MeV for set A [46], resulting in the sp levels of $0g_{9/2}$, $2s_{1/2}$, and $1d_{5/2}$ order. In Fig. 1, both sets exhibit similar sp energy dependence as a function of V_1, though the value of V_1 for set B tends to be stronger than that for set A to make $0g_{9/2}$ and $2s_{1/2}$ states

degenerate due to more diffused nuclear surface. To fix the range of V_1, the following two extreme cases are considered:

Vanishing spin-orbit limit. In Ref. [37], the $1d_{5/2}$ and $0g_{9/2}$ sp energies of ^{61}Ca are predicted to be 1.14 and 2.29 MeV. To realize this situation, we need to take a very small V_1 value, $V_1 \approx 0$ for set A and ≈ 5 MeV for set B, respectively. We call this choice of V_1 the vanishing spin-orbit (so) limit.

Degenerate sg limit. The sp energies of the $2s_{1/2}$ and $0g_{9/2}$ orbits are degenerate at $V_1 = 11.40$ MeV for set A and at $V_1 = 21.09$ MeV for set B. This choice of V_1 is called the degenerate sg limit. Despite both sp energies being the same, their respective root-mean-square (rms) radii are quite different: 36.0 and 5.04 fm for the $2s_{1/2}$ and $0g_{9/2}$ orbits of set A, and 36.1 and 5.28 fm for these orbits of set B. In both sets, the halo features are noticed in the s states, while the rms radii shrink significantly for the g states due to the $l = 4$ centrifugal barrier.

We examine the energy spectrum of ^{62}Ca by varying V_1 between the vanishing and degenerate limits. As the outcomes of both sets A and B are qualitatively the same, we discuss the results obtained with set A, unless otherwise mentioned.

B. Tests of FFLPG expansion

Before discussing the structure of ^{62}Ca, we evaluate the power of the FFLPG approach. We use the Minnesota (MN) potential [48] for v_{12} of Eq. (1). The MN potential, a soft-core central potential, is designed to reasonably well reproduce the energies and sizes of s-shell nuclei [28]. Since the two neutrons should be antisymmetric in the spin-orbital space, it is expected that they gain the attraction mostly in the relative s-wave and spin-singlet state. The spin-orbit and tensor components of v_{12} are therefore expected to play an insignificant role in the core$+n+n$ model. Refer to Refs. [49–51] for an example of demonstrating that the MN potential gives similar results as the realistic n-n ones.

Let L denote the relative orbital angular momentum between the two neutrons. The MN potential in the spin-singlet and even L channel reads $200e^{-1.487r^2} - 91.85e^{-0.405r^2}$ in MeV, where r is the two-nucleon distance in fm. For the spin-triplet and odd L channel it is given by $(200e^{-1.487r^2} - 178e^{-0.639r^2})(u - 1)$, where u is a parameter and usually taken to be around 1. In what follows, u is set to 1 and no interaction acts between the two neutrons in the spin-triplet and odd L channel.

To demonstrate the power of the FFLPG approach, we focus on such a state that is dominated by the weakly bound $2s_{1/2}$ orbit because the approach is expected to have the advantage in describing nodal orbits properly. We use the set A potential with $V_1 = 0$ and include the LPG bases restricted to $l_1 = l_2 = 0$. Figure 2 plots the energy as a function of K, for different choices of $k_{\max}$. The candidates for the basis states are generated randomly in the interval [0.1, 40] fm for $b = 1/\sqrt{a}$ and in the interval [0, $k_{\max}$] for k, and the best one is selected by the SVM algorithm. The results with the pseudopotential method are also shown for comparison. The FFLPG approach significantly improves the energy convergence. We confirm that $k_{\max} = 4$ truncation virtually gives the same curve as the one with $k_{\max} = 3$. The FFLPG calculation leads
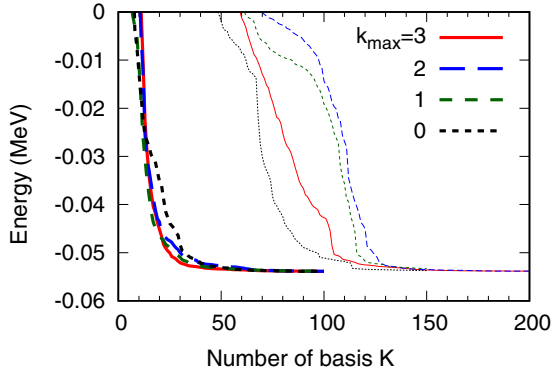
FIG. 2. Energy convergence of the ^{60}Ca $+n+n$ system with $J^\pi = 0^+$ as a function of the number of basis K. The calculations are performed only with $l_1 = l_2 = 0$ channel. Thick lines are the results with FFLPG functions, while thin lines are those with the pseudopotential method. See text for details.

to convergence within a few tens of basis functions, while the pseudopotential method needs more than a hundred bases to reach convergence. As for the pseudopotential method, it appears that the convergence is fastest when the ordinary Gaussians with $k_{max} = 0$ are used, and there is no significant advantage in using the LPG bases with $k_{max} > 0$. Probably this occurs because the $k = 0$ bases have the largest overlap with the $0s_{1/2}$ and $1s_{1/2}$ forbidden states, with the orthogonality requirement being most efficiently met by a superposition of those ordinary Gaussians. However, the energy obtained with $K = 150$ is -0.0537 for $k_{max} = 0$ and -0.0533 MeV for $k_{max} = 1$, respectively, which still misses the FFLPG energy of -0.0539 MeV. What is more serious in the pseudopotential method is its numerical instability. Because the $k = 0, 1$ bases have in general large overlap with the forbidden states, the calculation becomes numerically unstable due to the large prefactor λ in Eq. (14). It is very hard to extend the basis size without breaking the linear independence of the selected bases. With $k_{max} = 2, 3$ this instability problem is recovered and we get the energy of -0.0539 MeV by the pseudopotential method with $K = 200$.

Here, we should make a comment on the role of k in the LPG basis. As shown above, the FFLPG basis with $k_{max} > 0$ accelerates the energy convergence compared to the ordinary Gaussians with $k = 0$. To understand the reason, we plot in Fig. 3 the s-wave radial functions with different k values for some choices of a. The thick curves are for $\bar{\phi}_{k0}^a$ in Eq. (11), while the thin curves are for ϕ_{k0}^a that in general contains forbidden states. Note that the forbidden states are ψ_{00}^ν and ψ_{10}^ν. In the case of $b = 1/\sqrt{\nu} \equiv b_0$ the FFLPG function thus vanishes for $k = 0$ and 1, whereas it has two nodes at short distances for $k = 2$ and 3 because it is orthogonal to the forbidden states. With increasing b, the amplitude of the FFLPG function becomes smaller in the inner region and finally has no node for $k = 3$ at $b = 2.5b_0$ due to small overlap with the forbidden states. The FFLPG basis with $k = 0$ has small amplitude beyond the nuclear surface. With increasing k, however, it has large amplitude beyond the nuclear surface and damped amplitude at short distances. This property meets the
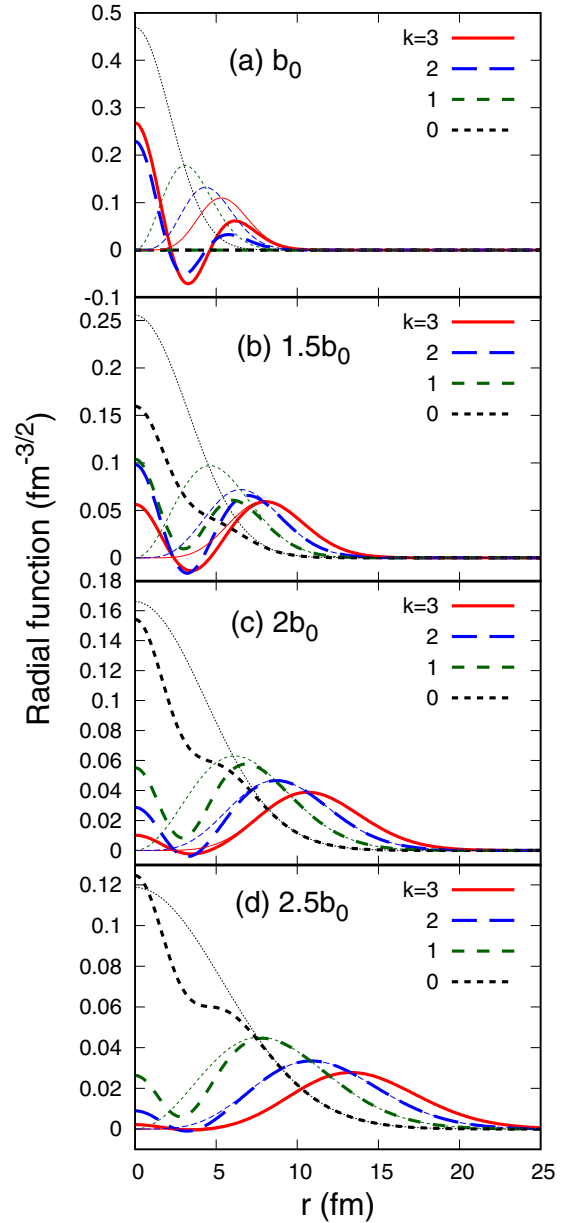

FIG. 3. s-wave radial functions of FFLPG $\bar{\phi}_{k0}^a$ (thick curves) and LPG ϕ_{k0}^a (thin curves) for different k values. The width parameter $b = 1/\sqrt{a}$ is chosen to be (a) b_0, (b) $1.5\,b_0$, (c) $2\,b_0$, and (d) $2.5\,b_0$, where $b_0 = 1/\sqrt{\nu} = 2.17$ fm with ν being the HO parameter of the forbidden states for ^{60}Ca $+n$.

requirement needed for the neutron orbits around the core nucleus and offers the possibility of efficiently describing neutron orbits with large radial extension. The FFLPG basis is also advantageous to gain the energy from the two-neutron interaction because it can have large relative s-wave components around the nuclear surface.

C. Application to ^{62}Ca

The test example presented in the previous subsection confirms that the FFLPG offer much faster and numerically stabler results than the pseudopotential method. In this
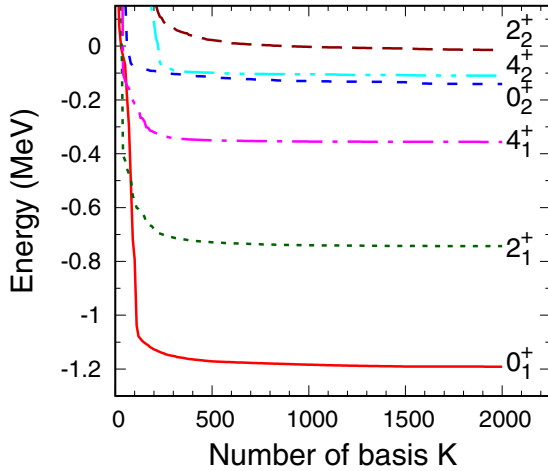
FIG. 4. Energies of $J^\pi = 0^+, 2^+,$ and 4^+ states of ^{62}Ca as a function of the number of basis K. The energy drawn is from the two-neutron threshold, and the spin-orbit strength is $V_1 = 11.40$ MeV, set A of the degenerate sg limit.

subsection, we study the structure of ^{62}Ca in the ^{60}Ca $+n + n$ model using the FFLPG expansion. We take $k_{max} = 3$ and $l_{max} = 10$ and generate the Gaussian falloff parameter $b = 1/\sqrt{a}$ in the interval [0.1,40] fm. All possible different combinations of (l_1, j_1) and (l_2, j_2) are taken into account. For example, the numbers of combinations are respectively 21, 55, and 69 for $J^\pi = 0^+, 2^+,$ and 4^+ states.

We exhibit in Fig. 4 the energies of the states with $J^\pi = 0^+, 2^+,$ and 4^+ as a function of K. The spin-orbit strength is $V_1 = 11.40$ MeV, set A of the degenerate sg limit. Note that the energy converges rapidly on a few hundred bases for all the states. This is because all the bases are made free from the forbidden states. The fourth digit of the energy does not change on $K = 1500$ for these lowest states. The second bound states are found for the $0^+, 2^+,$ and 4^+ states. We further increase the number of basis to lower the second bound states and confirm that they converge very well at $K = 2000$.

The truncation of $l_{max} = 10$ appears considerably large. One might question why so large a value is needed. Most of the sp levels are unbound in the present case, that is, they are nonresonant continuum states. The large value of l_{max} therefore suggests the need to account of the continuum effect to bind the two neutrons. Table I lists the l_{max} dependence of the basic properties of the 0_1^+ and 0_2^+ states. As the table indicates clearly, ϵ_{2n} increases, while $\langle v_{12} \rangle$ gets more attractive as a function of l_{max}. The l_{max} dependence of the two-neutron rms distance, r_{12}, shows an apparent correlation with $\langle v_{12} \rangle$. Although we confirm that the truncation with $l_{max} = 10$ takes into account most of the continuum effect, it appears that there may be still some room to improve the convergence by increasing l_{max} further.

In addition to the six states drawn in Fig. 4, we obtain two bound states with 6^+ and 8^+. Table II summarizes the energies, the rms neutron radii, and the occupation probabilities for those bound states. Note that the $0g_{9/2}$ and $2s_{1/2}$ sp states are set to be degenerate. The ground state exhibits nonhalo structure, occupying the $(g_{9/2})^2$ configuration by 94%. The

TABLE I. l_{max} dependence of the properties of two 0^+ states. E is the energy from the ^{60}Ca $+n+n$ threshold, $\epsilon_{2n} = \langle \sum_{i=1}^{2}(T_i + U_i) \rangle$ is the sum of the two-neutron sp energies, and $r_{12} = \sqrt{\langle (r_1 - r_2)^2 \rangle}$ is the rms relative distance between the two neutrons. Energy is in units of MeV and length is in units of fm.

	l_{max}	4	6	8	10
0_1^+	E	−0.99	−1.13	−1.16	−1.19
	ϵ_{2n}	0.14	0.33	0.38	0.43
	$\langle v_{12} \rangle$	−1.13	−1.39	−1.47	−1.55
	r_{12}	7.10	6.85	6.84	6.84
0_2^+	E	−0.10	−0.12	−0.14	−0.14
	ϵ_{2n}	0.17	0.27	0.33	0.35
	$\langle v_{12} \rangle$	−0.27	−0.39	−0.45	−0.48
	r_{12}	19.6	18.0	17.3	17.1

configuration also produces the $2_1^+, 4_1^+, 6^+,$ and 8^+ bound states that have almost the same structure as the ground state. Halo structure is realized as the 0_2^+ and 4_2^+ states. Both states have the rms neutron radius, r_{2n}, larger than 10 fm. As shown by the occupation probability, the 0_2^+ state may be called an s-wave two-neutron halo. It should be noted, however, that its r_{2n} value of about 13 fm is by far smaller than the rms radius of the $2s_{1/2}$ sp orbit, which is about 36 fm. This dramatic reduction is of course due to the correlated motion of the two neutrons. The one-neutron halo character of the 4_2^+ state is brought about by the coupling of the $g_{9/2}$ neutron with the $s_{1/2}$ neutron, as revealed by the occupation probabilities. This suggests that both states of two- and one-neutron halo structure can coexist within a narrow energy spacing. Despite the fact that it is barely bound, the 2_2^+ state shows no characteristics of halo structure. Its r_{2n} value is considerably large, 6.77 fm, but it is by far smaller than those of the 0_2^+ and 4_2^+ states. This is because the main configuration of the 2_2^+ state is $(g_{9/2}d_{5/2})$. Note that the recoil kinetic energy is not negligible as the binding energy is small.

Table II also lists the decomposition of the energy E into the sp energy, the recoil kinetic energy, the two-neutron interaction energy, and the rms two-neutron distance. The positive value of ϵ_{2n} indicates that the two neutrons move mostly in the continuum states. The recoil kinetic energies are small due to the factor $1/60m_N$. Clearly, the two-neutron interaction v_{12} plays a decisive role to make the two neutrons bound. At a closer look, the 2_2^+ state shows the largest sp energy and a relatively large energy gain from the two-neutron interaction energy. The state is realized by the coupling of the continuum states such as the $d_{5/2}$ and other high l orbits due to the two-neutron correlation.

The $(g_{9/2})^2$ dominance in the ground state can be explained by the pairing antihalo effect pointed out in Ref. [16]. A combination of the higher angular momentum states is more advantageous to gain energy from the pairing. In fact, $\langle v_{12} \rangle$ values are −1.55 and −0.48 MeV for 0_1^+ and 0_2^+, respectively. To make the ground state a halo, the energy difference between the $2s_{1/2}$ and $0g_{9/2}$ orbits should be sufficiently larger than the energy gain of the two-neutron interaction with the $(g_{9/2})^2$ configuration.

TABLE II. Properties of the spectrum of ^{62}Ca. The sp energies of $2s_{1/2}$ and $0g_{9/2}$ orbits are set to be -10 keV using the parameters of the degenerate sg limit of set A. The sp energy of the $1d_{5/2}$ orbit is 0.77 MeV. See Table I for the definitions of E, ϵ_{2n}, and r_{12}. $r_{2n} = \sqrt{\langle \frac{1}{2}(r_1^2 + r_2^2) \rangle}$ is the rms neutron radius, and $\langle T_{\text{rec}} \rangle = \langle \frac{1}{60m_N} \boldsymbol{p}_1 \cdot \boldsymbol{p}_2 \rangle$ is the recoil kinetic energy. P_{xy} denotes the occupation probability of finding x, y sp orbits, where x and y stand for $s_{1/2}$, $g_{9/2}$, $d_{5/2}$, respectively, and $\Delta P = 1 - \sum_{xy} P_{xy}$.

J^π	E (MeV)	r_{2n} (fm)	P_{ss}	P_{gg}	P_{dd}	P_{sg}	P_{sd}	P_{gd}	ΔP	ϵ_{2n} (MeV)	$\langle T_{\text{rec}} \rangle$ (MeV)	$\langle v_{12} \rangle$ (MeV)	r_{12} (fm)
0_1^+	-1.19	5.08	0.01	0.94	0.02				0.02	0.43	-0.07	-1.55	6.84
2_1^+	-0.74	5.12		0.86	0.01		0.01	0.09	0.03	0.40	-0.06	-1.08	6.96
4_1^+	-0.36	5.35		0.87	0.00	0.09		0.03	0.01	0.14	-0.03	-0.47	7.43
6^+	-0.22	5.03		0.99				0.01	0.01	0.04	-0.02	-0.24	7.05
8^+	-0.21	5.02		0.99					0.01	0.06	-0.01	-0.26	7.06
0_2^+	-0.14	12.8	0.91	0.02	0.05				0.03	0.35	-0.01	-0.48	17.1
4_2^+	-0.11	10.1		0.10	0.00	0.87		0.02	0.01	0.08	-0.01	-0.18	14.3
2_2^+	-0.014	6.77		0.13	0.03		0.14	0.64	0.06	1.04	-0.04	-1.02	9.09

As mentioned above, the 4_2^+ state is found to have one-neutron halo structure constructed dominantly from the $(s_{1/2}g_{9/2})$ configuration. That configuration would suggest a doublet state with 5^+. However, its dominant configuration is in the spin-triplet and odd L channel. Possible existence of this unnatural-parity state crucially depends on the choice of u parameter. Since we set $u = 1$, v_{12} vanishes and no doublet state appears. To be more definitive about its existence, we have to test other realistic n-n potentials.

As discussed above, when the spin-orbit strength V_1 of the n-^{60}Ca potential is taken to be the degenerate sg limit, the $J^\pi = 0^+$ halo structure appears as the excited state. It is interesting to examine how the 0^+ state changes if the spin-orbit strength is weakened towards the vanishing so limit. We introduce a multiplicative factor f and set the spin-orbit strength as $V_1 = fV_1'$ ($0 \leqslant f \leqslant 1$) with $V_1' = 11.40$ MeV for set A. The limit of $f \approx 0$ is the case used in Ref. [37], where the energy difference between the $2s_{1/2}$ and $0g_{9/2}$ orbits is large (see Fig. 1) and only one bound state of two-neutron halo structure is predicted.

Figure 5(a) displays the energy of the 0^+ state as a function of f. Only one 0^+ state appears for $f < 0.7$ and the existence of the second 0^+ state is possible for $f \geqslant 0.7$. Figure 5(b) shows the corresponding rms neutron radii. The halo structure having a radius larger than 10 fm emerges in the ground state for $f < 0.7$. For $f > 0.7$ the 0_2^+ state exhibits the two-neutron halo structure, whereas the ground state turns out to be a compact state. At $f = 0.7$ the ground state shows intermediate structure between halo and compact states. The rms radius of the 0_2^+ state is extremely large due to the small binding energy of -0.03 MeV. This behavior can be understood by showing the occupation probabilities. Figure 5(c) shows the occupation probabilities of finding $(s_{1/2})^2$ and $(g_{9/2})^2$ components in the 0^+ states. The contributions of $(d_{5/2})^2$ component for the 0_1^+ state are at most 0.09 at $f = 0.7$ and other contributions are less than 0.05 in total. For the 0_2^+ state, those contributions are less about 0.01. As expected, the $(s_{1/2})^2$ component dominates in the ground state at $f = 0$, resulting in a large rms radius of 12 fm, almost the same structure as the 0_2^+ state at $f = 1$. By increasing f, i.e., reducing the energy difference between the $2s_{1/2}$ and $0g_{9/2}$ orbits, the occupation probability of the $0g_{9/2}$ orbit increases gradually and rises suddenly for

$f > 0.6$. The rms radius decreases simultaneously with the growing occupation of the $0g_{9/2}$ orbit that has a much smaller radius. An almost equal mixing of the $(s_{1/2})^2$ and $(g_{9/2})^2$ configurations occurs at $f = 0.7$. Here the energy difference
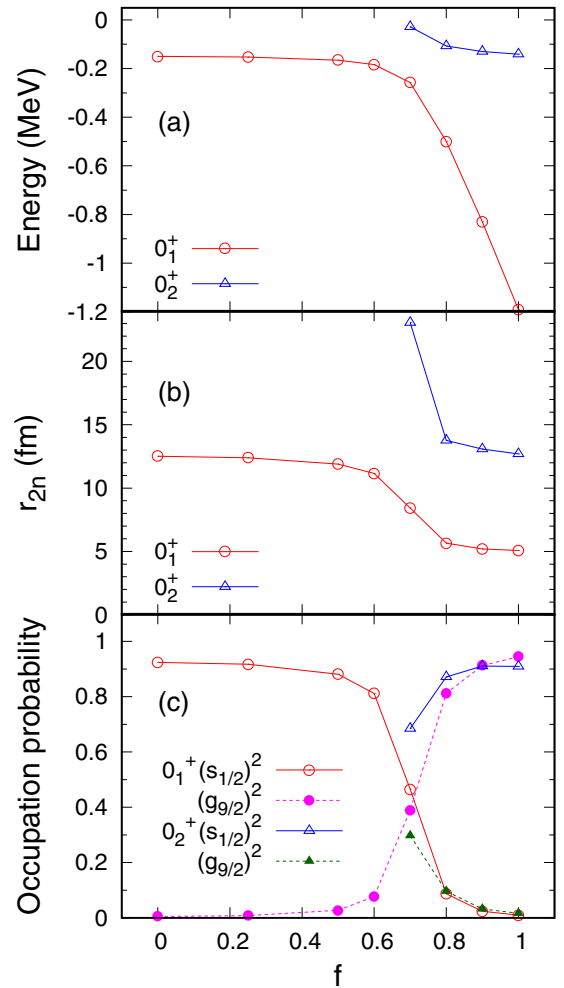

FIG. 5. (a) Energies, (b) rms two-neutron radii, and (c) occupation probabilities of the 0_1^+ and 0_2^+ states of ^{62}Ca as a function of f. The spin-orbit strength is taken to be $V_1 = fV_1'$ with $V_1' = 11.40$ MeV for set A.

between the $2s_{1/2}$ and $0g_{9/2}$ orbit is approximately 0.5 MeV, which is comparable to the difference of $\langle v_{12} \rangle / 2$ for the two 0^+ states as shown in Table II. Finally, the ground state becomes $g_{9/2}$ dominant at $f = 1$, where the sp energies of the $2s_{1/2}$ and $0g_{9/2}$ orbits are degenerate, while the 0_2^+ state exhibits two-neutron halo structure consisting of the $(s_{1/2})^2$ configuration.

D. Probable halo ground state of ^{72}Ca

An extension to the ^{70}Ca $+ n + n$ model is straightforward. The reader is referred to Ref. [19] for the structure of ^{72}Ca by the hyperspherical method. We follow the case of ^{62}Ca starting from discussing some constraints on the phenomenological WS potential parameters.

The n-^{70}Ca potential should bind the $0g_{9/2}$ orbit due to the assumption of the $N = 50$ core. However, no bound $0g_{9/2}$ orbit is generated if we assume the parametrization of Ref. [46]. Instead of searching for such a potential that binds the $0g_{9/2}$ orbit, we simply assume that all the occupied neutron orbits including the $0g_{9/2}$ orbit are described by the HO functions with the oscillator parameter ν' that is scaled from the ^{60}Ca parameter ν by $\nu' = (60/70)^{1/3}\nu$. The sp energy spectrum of ^{71}Ca with respect to V_1 is virtually the same as Fig. 1 except for the absence of the $0g_{9/2}$ level.

To bind the $2s_{1/2}$ orbit at -0.01 MeV, the strength V_0 turns out to be 40.26 MeV for set A and 38.32 MeV for set B. Since V_0 gets weaker than the ^{60}Ca-n case, we have only one bound 0^+ state that has two-neutron halo structure if V_1 is taken to be the same as that of ^{61}Ca: The energy, rms neutron radius, and $(s_{1/2})^2$ and $(d_{5/2})^2$ occupation probabilities are -0.14 MeV, 12.7 fm, and 0.89 and 0.08 for set A, whereas for set B they are -0.13 MeV, 13.3 fm, and 0.87 and 0.11, respectively. The n-^{70}Ca potential used here makes the energy gap between the $2s_{1/2}$ and $1d_{5/2}$ orbits too large to mix those sp states. To make the $1d_{5/2}$ orbit bound is very unlikely because V_1 has to be taken more than two times larger than the standard value. Within the present phenomenological n-^{70}Ca potential, the halo structure emerges if the energy of the $2s_{1/2}$ state is close to zero, which is the same conclusion drawn in Ref. [19].

IV. CONCLUSIONS AND PROSPECTS

We have developed a forbidden-state-free locally peaked Gaussian expansion method to describe the weakly bound correlated neutron motion around a heavy core. The power of this approach has been tested by taking examples of the weakly bound three-body systems ^{60,70}Ca $+ n + n$. The expansion proposed here accelerates the energy convergence much

faster and offers numerically by far stabler results than the pseudopotential projection method [24]. The present method allows us to predict very weakly bound excited states. The energy spectra of unknown ^{62,72}Ca have been calculated to discuss the possibility of halo-structure emergence by varying the single-particle levels of unknown ^{60,70}Ca $+ n$ systems.

In the extreme single-particle level ordering of $2s_{1/2}$, $1d_{5/2}$, and $0g_{9/2}$ orbits predicted by Ref. [37], only one bound state is found in ^{62}Ca, exhibiting s-wave two-neutron halo structure. The emergence of the halo structure in the ground state in fact strongly depends on the energy difference between the $2s_{1/2}$ and $0g_{9/2}$ orbits for ^{62}Ca and between the $2s_{1/2}$ and $1d_{5/2}$ orbits for ^{72}Ca. Under the very limited condition that the $2s_{1/2}$ and $0g_{9/2}$ orbits are bound and degenerate, however, the ground state becomes a 0^+ nonhalo state dominated by the $0g_{9/2}$ orbit, consistent with the pairing antihalo effect [16]. In that case, a 0^+ two-neutron halo state appears slightly above the ground state. In addition a 4^+ one-neutron halo state appears at almost the same excitation energy as the 0^+ excited state. Apparently experimental information on the single-neutron levels of ^{60,70}Ca $+ n$ system is crucially important to identify the structure of these neutron-rich Ca isotopes.

The method proposed here can straightforwardly be extended to core plus more-nucleon systems. Since it is advantageous to describe localized orbits near the surface of the core, it is interesting to apply the method for alpha-decay phenomena of heavy nuclei. The result of Ref. [30] for the ^{212}Po problem could be improved with locally peaked Gaussians. A systematic analysis of the degree of the alpha clustering near the nuclear surface is interesting as it has recently been realized in alpha-knockout reactions on Sn isotopes [52].

[1] D. S. Ahn, N. Fukuda, H. Geissel, N. Inabe, N. Iwasa, T. Kubo, K. Kusaka, D. J. Morrissey, D. Murai, T. Nakamura, M. Ohtake, H. Otsu, H. Sato, B. M. Sherrill, Y. Shimizu, H. Suzuki, H. Takeda, O. B. Tarasov, H. Ueno, Y. Yanagisawa, and K. Yoshida, Phys. Rev. Lett. **123**, 212501 (2019).

[2] I. Tanihata, H. Hamagaki, O. Hashimoto, Y. Shida, N. Yoshikawa, K. Sugimoto, O. Yamakawa, T. Kobayashi, and N. Takahashi, Phys. Rev. Lett. **55**, 2676 (1985).

[3] I. Tanihata, T. Kobayashi, O. Yamakawa, S. Shimoura, K. Ekuni, K. Sugimoto, N. Takahashi, T. Shimoda, and H. Sato, Phys. Lett. B **206**, 592 (1988).

[4] T. Suzuki, R. Kanungo, O. Bochkarev, L. Chulkov, D. Cortina, M. Fukuda, H. Geissel, M. Hellström, M. Ivanov, R. Janik *et al.*, Nucl. Phys. A **658**, 313 (1999).

[5] W. Horiuchi and Y. Suzuki, Phys. Rev. C **74**, 034311 (2006).

[6] K. Tanaka, T. Yamaguchi, T. Suzuki, T. Ohtsubo, M. Fukuda, D. Nishimura, M. Takechi, K. Ogata, A. Ozawa, T. Izumikawa, T. Aiba, N. Aoi, H. Baba, Y. Hashizume, K. Inafuku, N. Iwasa, K. Kobayashi, M. Komuro, Y. Kondo, T. Kubo *et al.*, Phys. Rev. Lett. **104**, 062701 (2010).

[7] Y. Togano, T. Nakamura, Y. Kondo, J. A. Tostevin, A. T. Saito, J. Gibelin, N. A. Orr, N. L. Achouri, T. Aumann, H. Baba *et al.*, Phys. Lett. B **761**, 412 (2016).

[8] I. Tanihata, H. Savajols, and R. Kanungo, Prog. Part. Nucl. Phys. **68**, 215 (2013), and references therein.

[9] S. Bagchi, R. Kanungo, Y. K. Tanaka, H. Geissel, P. Doornenbal, W. Horiuchi, G. Hagen, T. Suzuki, N. Tsunoda, D. S. Ahn, H. Baba, K. Behr, F. Browne, S. Chen, M. L. Cortes, A. Estrade, N. Fukuda, M. Holl, K. Itahashi *et al.*, Phys. Rev. Lett. **124**, 222504 (2020).

[10] V. N. Efimov, Phys. Lett. B **33**, 563 (1970).

[11] D. V. Fedorov, A. S. Jensen, and K. Riisager, Phys. Rev. Lett. **73**, 2817 (1994).

[12] T. Frederico, A. Delfino, L. Tomio, and M. T. Yamashita, Prog. Part. Nucl. Phys. **67**, 939 (2012).

[13] J. Singh, J. Casal, W. Horiuchi, L. Fortunato, and A. Vitturi, Phys. Rev. C **101**, 024310 (2020).

[14] L. Fortunato, J. Casal, W. Horiuchi, J. Singh, and A. Vitturi, Commun. Phys. **3**, 132 (2020).

[15] J. Casal, J. Singh, L. Fortunato, W. Horiuchi, and A. Vitturi, Phys. Rev. C **102**, 064627 (2020).

[16] H. Masui, W. Horiuchi, and M. Kimura, Phys. Rev. C **101**, 041303(R) (2020).

[17] N. Michel, J. G. Li, F. R. Xu, and W. Zuo, Phys. Rev. C **101**, 031301(R) (2020).

[18] G. Hagen, P. Hagen, H.-W. Hammer, and L. Platter, Phys. Rev. Lett. **111**, 132501 (2013).

[19] D. Hove, E. Garrido, P. Sarriguren, D. V. Fedorov, H. O. U. Fynbo, A. S. Jensen, and N. T. Zinner, Phys. Rev. Lett. **120**, 052502 (2018).

[20] M. A. Shalchi, M. T. Yamashita, M. R. Hadizadeh, E. Garrido, L. Tomio, and T. Frederico, Phys. Rev. A **97**, 012701 (2018).

[21] J. P. Incao, J. Phys. B: At. Mol. Opt. Phys. **51**, 043001 (2018).

[22] S. Saito, Prog. Theor. Phys. **40**, 893 (1968).

[23] S. Saito, Prog. Theor. Phys. **62**, 11 (1977).

[24] V. I. Kukulin and V. N. Pomerantsev, Ann. Phys. (NY) **111**, 330 (1978).

[25] K. Varga and Y. Suzuki, Phys. Rev. C **52**, 2885 (1995).

[26] Y. Suzuki and K. Varga, *Stochastic Variational Approach to Quantum-Mechanical Few-Body Problems*, Lecture Notes in Physics Vol. 54 (Springer, Berlin, 1998).

[27] J. Mitroy, S. Bubin, W. Horiuchi, Y. Suzuki, L. Adamowicz, W. Cencek, K. Szalewicz, J. Komasa, D. Blume, and K. Varga, Rev. Mod. Phys. **85**, 693 (2013).

[28] Y. Suzuki, W. Horiuchi, M. Orabi, and K. Arai, Few-Body Syst. **42**, 33 (2008).

[29] W. Horiuchi and Y. Suzuki, Phys. Rev. C **89**, 011304(R) (2014).

[30] K. Varga and R. J. Liotta, Phys. Rev. C **50**, R1292(R) (1994).

[31] Y. Suzuki and W. Horiuchi, Phys. Rev. C **95**, 044320 (2017).

[32] Y. Suzuki, Phys. Rev. C **101**, 014002 (2020).

[33] O. B. Tarasov, D. S. Ahn, D. Bazin, N. Fukuda, A. Gade, M. Hausmann, N. Inabe, S. Ishikawa, N. Iwasa, K. Kawata, T. Komatsubara, T. Kubo, K. Kusaka, D. J. Morrissey, M. Ohtake, H. Otsu, M. Portillo, T. Sakakibara, H. Sakurai *et al.*, Phys. Rev. Lett. **121**, 022501 (2018).

[34] S. Michimasa, M. Kobayashi, Y. Kiyokawa, S. Ota, D. S. Ahn, H. Baba, G. P. A. Berg, M. Dozono, N. Fukuda, T. Furuno, E. Ideguchi, N. Inabe, T. Kawabata, S. Kawase, K. Kisamori, K. Kobayashi, T. Kubo, Y. Kubota, C. S. Lee *et al.*, Phys. Rev. Lett. **121**, 022506 (2018).

[35] R. F. Garcia Ruiz, M. L. Bissell, K. Blaum, A. Ekström, N. Frömmgen, G. Hagen, M. Hammen, K. Hebeler, J. D. Holt, G. R. Jansen *et al.*, Nat. Phys. **12**, 594 (2016).

[36] M. Tanaka, M. Takechi, M. Fukuda, D. Nishimura, T. Suzuki, Y. Tanaka, T. Moriguchi, D. S. Ahn, A. Aimaganbetov, M. Amano *et al.*, Phys. Rev. Lett. **124**, 102501 (2020).

[37] G. Hagen, M. Hjorth-Jensen, G. R. Jansen, R. Machleidt, and T. Papenbrock, Phys. Rev. Lett. **109**, 032502 (2012).

[38] J. Erler, N. Birge, M. Kortelainen, W. Nazarewicz, E. Olsen, A. M. Perhac, and M. Stoitsov, Nature (London) **486**, 509 (2012).

[39] C. Forssén, G. Hagen, M. Hjorth-Jensen, W. Nazarewicz, and J. Rotureau, Phys. Scr. T **152**, 014022 (2013).

[40] L. Coraggio, G. De Gregorio, A. Gargano, N. Itaco, T. Fukui, Y. Z. Ma, and F. R. Xu, Phys. Rev. C **102**, 054326 (2020).

[41] S. R. Stroberg, J. D. Holt, A. Schwenk, and J. Simonis, Phys. Rev. Lett. **126**, 022501 (2021).

[42] J. Meng, H. Toki, J. Y. Zeng, S. Q. Zhang, and S.-G. Zhou, Phys. Rev. C **65**, 041302(R) (2002).

[43] L. Neufcourt, Y. Cao, W. Nazarewicz, E. Olsen, and F. Viens, Phys. Rev. Lett. **122**, 062502 (2019).

[44] Y. Suzuki and K. Ikeda, Phys. Rev. C **38**, 410 (1988).

[45] Y. Suzuki and W. Horiuchi, in *Emergent Phenomena in Atomic Nuclei from Large-scale Modeling: A Symmetry-Guided Perspective* (World Scientific, Singapore, 2017), Chap. 7, pp. 199–227.

[46] A. Bohr and B. R. Mottelson, *Nuclear Structure, Vol. I* (W. A. Benjamin, New York, 1975).

[47] W. Horiuchi, Y. Suzuki, B. Abu-Ibrahim, and A. Kohama, Phys. Rev. C **75**, 044607 (2007).

[48] D. R. Thompson, M. LeMere, and Y. C. Tang, Nucl. Phys. A **286**, 53 (1977).

[49] Y. Suzuki, H. Matsumura, and B. Abu-Ibrahim, Phys. Rev. C **70**, 051302(R) (2004).

[50] W. Horiuchi and Y. Suzuki, Phys. Rev. C **73**, 037304 (2006); **74**, 019901(E) (2006).

[51] W. Horiuchi and Y. Suzuki, Phys. Rev. C **76**, 024311 (2007).

[52] J. Tanaka, Z. H. Yang, S. Typel, S. Adachi, S. Bai, P. van Beek, D. Beaumel, Y. Fujikawa, J. Han, S. Heil *et al.*, Science **371**, 260 (2021).